



Cite this: *Chem. Sci.*, 2024, **15**, 307

All publication charges for this article have been paid for by the Royal Society of Chemistry

Received 22nd October 2023  
Accepted 24th November 2023

DOI: 10.1039/d3sc05623f  
[rsc.li/chemical-science](http://rsc.li/chemical-science)

## Photocatalytic ethane conversion on rutile $\text{TiO}_2(110)$ : identifying the role of the ethyl radical<sup>†</sup>

Fangliang Li, <sup>‡a</sup> Yuemiao Lai, <sup>‡a</sup> Yi Zeng, <sup>‡a</sup> Xiao Chen, <sup>a</sup> Tao Wang, <sup>a</sup> Xueming Yang <sup>abc</sup> and Qing Guo <sup>\*a</sup>

Oxidative dehydrogenation of ethane ( $\text{C}_2\text{H}_6$ , ODHE) is a promising approach to producing ethene ( $\text{C}_2\text{H}_4$ ) in the chemical industry. However, the ODHE needs to be operated at a high temperature, and realizing the ODHE under mild conditions is still a big challenge. Herein, using photocatalytic ODHE to obtain  $\text{C}_2\text{H}_4$  has been achieved successfully on a model rutile(R)- $\text{TiO}_2(110)$  surface with high selectivity. Initially, the  $\text{C}_2\text{H}_6$  reacts with hole trapped  $\text{O}_{\text{Ti}}^-$  centers to produce ethyl radicals ( $\text{C}_2\text{H}_5^{\cdot}$ ), which can be precisely detected by a sensitive TOF method, and then the majority of the  $\text{C}_2\text{H}_5^{\cdot}$  radicals spontaneously dehydrogenate into  $\text{C}_2\text{H}_4$  without another photo-generated hole. In addition, parts of the  $\text{C}_2\text{H}_5^{\cdot}$  radicals rebound with diversified surface sites to produce  $\text{C}_2$  products via migration along the surface. The mechanistic model built in this work not only advances our knowledge of the C–H bond activation and low temperature  $\text{C}_2\text{H}_6$  conversion, but also provides new opportunities for realizing the ODHE with high  $\text{C}_2\text{H}_4$  efficiency under mild conditions.

## Introduction

Ethene ( $\text{C}_2\text{H}_4$ ), as an important basic material for manufacturing diverse consumer products, accounts for about 75% of petrochemical products.<sup>1,2</sup> With the increase of global  $\text{C}_2\text{H}_4$  demand, environmental and economic issues have become serious problems facing the world because of the energy- and emission-intensive activities for  $\text{C}_2\text{H}_4$  production (e.g., naphtha steam cracking,<sup>3–5</sup> fluidized catalytic cracking (FCC),<sup>6–8</sup> methanol-to-olefins (MTO)<sup>2</sup> and Fischer–Tropsch to olefins (FTO)<sup>2</sup>). The vigorous exploitation of shale gas containing abundant light alkanes has promoted the development of the direct dehydrogenation of ethane ( $\text{C}_2\text{H}_6$ ) to  $\text{C}_2\text{H}_4$ . However, compared with the non-oxidative dehydrogenation of the  $\text{C}_2\text{H}_6$  technique, which is thermodynamically limited with highly endothermic properties, the selective oxidative dehydrogenation (ODH) of  $\text{C}_2\text{H}_6$  is a promising alternative route for  $\text{C}_2\text{H}_4$  production due to its autothermal conditions.<sup>1,2,9,11</sup>

Although the ODH of  $\text{C}_2\text{H}_6$  (ODHE) is thermodynamically favored, it is still often conducted under harsh conditions (high temperature and pressure) because of the high chemical

stability of the C–H bonds (414 kJ mol<sup>–1</sup>), resulting in high energy consumption, catalyst deactivation, and over oxidation.<sup>1,2,10</sup> Therefore, various new catalysts (such as boron nitride (BN) based catalysts,<sup>12,13</sup> metal dopants<sup>14,15</sup>) and approaches (including  $\text{CO}_2$ -assisted oxidation,<sup>16,17</sup> chemical looping oxidative dehydrogenation (CL-ODH),<sup>18,19</sup> and so on) were developed to achieve the ODHE process with high selectivity and high efficiency under mild conditions. Among them, photocatalysis, as an emerging technology, can efficiently utilize clean solar energy for the C–H bond activation under mild conditions. Recently, both theoretical and experimental results have shown that  $\text{TiO}_2$ -based catalysts have potential for C–H bond activation of light alkanes,<sup>20–25</sup> indicating that the photocatalytic ODHE may achieve selective  $\text{C}_2\text{H}_4$  production under mild conditions. Although both theoretical and experimental studies claimed that alkyl radical intermediates may be formed in the photocatalytic conversion of light alkanes,<sup>20–25</sup> the formation of alkyl radicals is rarely identified due to the sensitivity of the experimental methods, which have confused the fundamental understandings of these reactions. Therefore, illustrating the formation of the ethyl ( $\text{C}_2\text{H}_5^{\cdot}$ ) radical in photocatalytic ODHE could play a vital role in understanding the microkinetic mechanisms underlying the reaction.

Herein, we systematically investigated the use of photocatalytic ODHE with rutile- $\text{TiO}_2(110)$  using temperature-programmed desorption (TPD), photo stimulated desorption (PSD), and time-of-flight (TOF) methods. The results demonstrate that using photocatalytic ODHE to obtain  $\text{C}_2\text{H}_4$  can be achieved efficiently on the O atom covered R- $\text{TiO}_2(110)$  surface, and the  $\text{C}_2\text{H}_5^{\cdot}$  radical intermediate is captured very sensitively.

<sup>a</sup>Shenzhen Key Laboratory of Energy Chemistry & Department of Chemistry, Southern University of Science and Technology, Shenzhen, Guangdong 518055, PR China.  
E-mail: guoq@sustech.edu.cn

<sup>b</sup>State Key Laboratory of Molecular Reaction Dynamics, Dalian Institute of Chemical Physics, Chinese Academy of Sciences, Dalian, Liaoning 116023, PR China

<sup>c</sup>Hefei National Laboratory, Hefei 230088, PR China

<sup>†</sup> Electronic supplementary information (ESI) available. See DOI: <https://doi.org/10.1039/d3sc05623f>

<sup>‡</sup> These authors contributed equally to this work.



Furthermore, a clear insight into the microkinetic mechanism of the photocatalytic ODHE has been explored.

## Experimental

All the TPD experiments were performed with a home-built apparatus, which has been described in detail elsewhere.<sup>26</sup> The preparation of the well-ordered R-TiO<sub>2</sub>(110) crystal surfaces (Princeton Scientific, 10 mm × 10 mm × 1 mm) was accomplished using cycles of Ar<sup>+</sup> sputtering and annealing at 850 K in an ultra-high vacuum (UHV). The characterization of the ordering and cleanliness of the R-TiO<sub>2</sub>(110) surfaces was conducted using low-energy electron diffraction (LEED) and Auger electron spectroscopy (AES), respectively. The density of the oxygen vacancies (O<sub>v</sub>) on the surface was measured using H<sub>2</sub>O TPD, and was determined to be about 6–7%. The purity of the C<sub>2</sub>H<sub>6</sub> and O<sub>2</sub> gases used in the experiment was ≥99.99%. The 355 nm light was produced using a fiber laser (Braze Laser UV), and the pulse time and repetition rate of the laser were ≤15 ps and 400 kHz, respectively. The third harmonic (343 nm) output was produced from a 1030 nm laser (Flare NX laser, Coherent), and the pulse time and repetition rate of the UV laser were 1.5 ns and 200 Hz, respectively. To minimize the increase of surface temperature by the UV irradiation, the maximum power of the laser is 5 mW, corresponding to a flux of  $2.1 \times 10^{16}$  photons per cm<sup>2</sup> per s at 355 nm, and  $2.0 \times 10^{16}$  photons per cm<sup>2</sup> per s at 343 nm. During the UV light irradiation process, the temperature increase of the surface was less than 2 K. The previously described laser (Braze Laser UV) was used in photocatalytic reactions and the PSD measurements. In order to improve the signal-to-background ratio for sensitively detecting trace signals of the photo-desorbed products, the Flare NX laser (Coherent) was used in the TOF measurements.

For the PSD measurements, the time resolution was set to 0.5 s. If we assume that the ionization of the background residual gases under vacuum will produce  $1 \times 10^6$  counts per second (cps) at  $m/z = 29$ , and the ionization of the C<sub>2</sub>H<sub>5</sub> radical product will produce  $1 \times 10^5$  cps for C<sub>2</sub>H<sub>5</sub><sup>+</sup> ( $m/z = 29$ ), and the signal-to-noise ratio (SNR) the PSD method used here was 10 : 1. If the fluctuation of the signal of  $m/z = 29$  from the background was about 10%, it was hard to determine whether the C<sub>2</sub>H<sub>5</sub> radical had been produced. However, when the 200 Hz light was used for the experiment with a TOF analyzer, the moment that the laser light arrived at the surface was set as time zero, and the C<sub>2</sub>H<sub>5</sub><sup>+</sup> signal arriving at the detector could be precisely counted in an exact relationship to their arrival time in each pulse. The time interval between every laser shot was 5 ms, and the time resolution was set to 256 ns for the TOF measurements. The background signal of the C<sub>2</sub>H<sub>5</sub><sup>+</sup> signal was produced randomly, and then the background signal collected in each frequency bin was  $(1 \times 10^6 \div 200) \div (5 \text{ ms} \div 256 \text{ ns}) \approx 0.256$  count per 256 ns. However, the production of C<sub>2</sub>H<sub>5</sub> radical was not random, and it was produced at the time scale of 0.1 ms (see below). Correspondingly, the C<sub>2</sub>H<sub>5</sub><sup>+</sup> product signal collected in each frequency bin is  $(1 \times 10^5 \div 200) \div (0.1 \text{ ms} \div 256 \text{ ns}) \approx 1.28$  count per 256 ns, and the SNR of the TOF method was 1 : 5. As

a result, the sensitivity of the TOF method was much higher than that of the PSD method (10 : 1).

## Results

### The TPD results of the C<sub>2</sub>H<sub>6</sub> conversion into C<sub>2</sub>H<sub>4</sub>

Fig. 1 shows the typical TPD spectra of the mass-to-charge ratios ( $m/z$ ) of 15 (CH<sub>3</sub><sup>+</sup>), 18 (H<sub>2</sub>O<sup>+</sup>), 26 (C<sub>2</sub>H<sub>2</sub><sup>+</sup>), 27 (C<sub>2</sub>H<sub>3</sub><sup>+</sup>), 28 (C<sub>2</sub>H<sub>4</sub><sup>+</sup> and CO<sup>+</sup>), 29 (C<sub>2</sub>H<sub>5</sub><sup>+</sup> and CHO<sup>+</sup>), 30 (C<sub>2</sub>H<sub>6</sub><sup>+</sup>), 31 (CH<sub>2</sub>OH<sup>+</sup>) and 43 (CH<sub>3</sub>CO<sup>+</sup>) collected on the oxidized R-TiO<sub>2</sub>(110) surfaces after adsorbing 0.28 ML (1 ML =  $5.2 \times 10^{14}$  molecules per cm<sup>2</sup>) of C<sub>2</sub>H<sub>6</sub> followed by 355 nm irradiation for 0 (black lines) and 10 min (red lines). The oxidized R-TiO<sub>2</sub>(110) surfaces were prepared by exposing the reduced surfaces to 200 L of O<sub>2</sub> at 300 K.<sup>25,27,28</sup> After surface oxidation, the bridging oxygen vacancies (O<sub>v</sub>) will be healed, leaving oxygen atoms on the five coordinated Ti<sup>4+</sup> sites (Ti<sub>5c</sub>, O<sub>Ti</sub>).<sup>25</sup> Before irradiation, only one desorption peak at 129 K appeared in the TPD traces of  $m/z = 15, 26, 27, 28, 29, 30$ , and 31, which was attributed to the desorption of the molecular C<sub>2</sub>H<sub>6</sub> on the Ti<sub>5c</sub> sites (C<sub>2</sub>H<sub>6(Ti)</sub>).<sup>29</sup> No signals from thermocatalytic products suggested that the oxidized R-TiO<sub>2</sub>(110) surface was not thermally active for the C–H bond activation of C<sub>2</sub>H<sub>6</sub>.

After 355 nm irradiation, a new desorption peak at 330 K was observed in the TPD spectra of  $m/z = 18$  (Fig. 1a), which was contributed by the molecular H<sub>2</sub>O desorption on the Ti<sub>5c</sub> sites (H<sub>2</sub>O<sub>Ti</sub>) or recombinational H<sub>2</sub>O desorption from the terminal OH groups on the Ti<sub>5c</sub> sites (OH<sub>Ti</sub>).<sup>30</sup> The H atoms of the H<sub>2</sub>O product could only be from C<sub>2</sub>H<sub>6(Ti)</sub>, demonstrating that the photocatalytic dehydrogenation of C<sub>2</sub>H<sub>6(Ti)</sub> occurred on the O<sub>Ti</sub> atom covered R-TiO<sub>2</sub>(110) surface. Conversely, the reduced R-TiO<sub>2</sub>(110) showed no photoactivity for the ODHE process (see Fig. S1, ESI†). Based on our previous results of the photocatalytic oxidative dehydrogenation of propane (C<sub>3</sub>H<sub>8</sub>, ODHP) on R-TiO<sub>2</sub>(110),<sup>25</sup> the hole trapped O<sub>Ti</sub><sup>–</sup> centers rather than hole trapped bridging oxygen atoms (O<sub>b</sub><sup>–</sup>) were the active species for the initial C–H bond activation of C<sub>2</sub>H<sub>6</sub>, leading to the formation of H<sub>2</sub>O<sub>Ti</sub> and OH<sub>Ti</sub> (Fig. 1a).

The H<sub>2</sub>O<sub>Ti</sub> formation was accompanied by several desorption features of carbon-containing products, which were observed at 168 K, 365 K, 423 K, 580 K, and 585 K (Fig. 1b). The broad peak (400–700 K) in the TPD traces of  $m/z = 15, 26, 27, 28, 29$  and 30 was due to the desorption of C<sub>2</sub>H<sub>6</sub> from the copper blocks, which were used for the mounting tantalum sample holder (Fig. S2, ESI†). The relative intensity ratio of the 365 K peak in the TPD traces of  $m/z = 15, 29$ , and 43 were calculated to be 0.80 : 1 : 0 : 14, respectively, which was very close to that of acetaldehyde (CH<sub>3</sub>CHO) measured by mass spectrometry (Fig. S3, ESI†). Therefore, this peak could be attributed to the formation of CH<sub>3</sub>CHO on the Ti<sub>5c</sub> sites.<sup>31</sup> The tiny peak at 585 K ( $m/z = 31$ ) was likely to be due to the formation of ethanol (C<sub>2</sub>H<sub>5</sub>OH).<sup>32</sup> In addition, as shown in Fig. 1b, the relative intensities of the 168 K, 423 K, and 580 K peaks in the TPD traces of  $m/z = 26$  and 27 were calculated to be 0.87 : 1 (168 K), 0.89 : 1 (423 K) and 0.88 : 1 (580 K), respectively, which were very close to that of the C<sub>2</sub>H<sub>4</sub> sample (Fig. S4, ESI†), and very different from that of the alkanes and alkenes (C<sub>n</sub>H<sub>2n</sub> ( $3 \leq n \leq 10$ ) and C<sub>n</sub>H<sub>2n+2</sub> ( $2 \leq n \leq 10$ )).



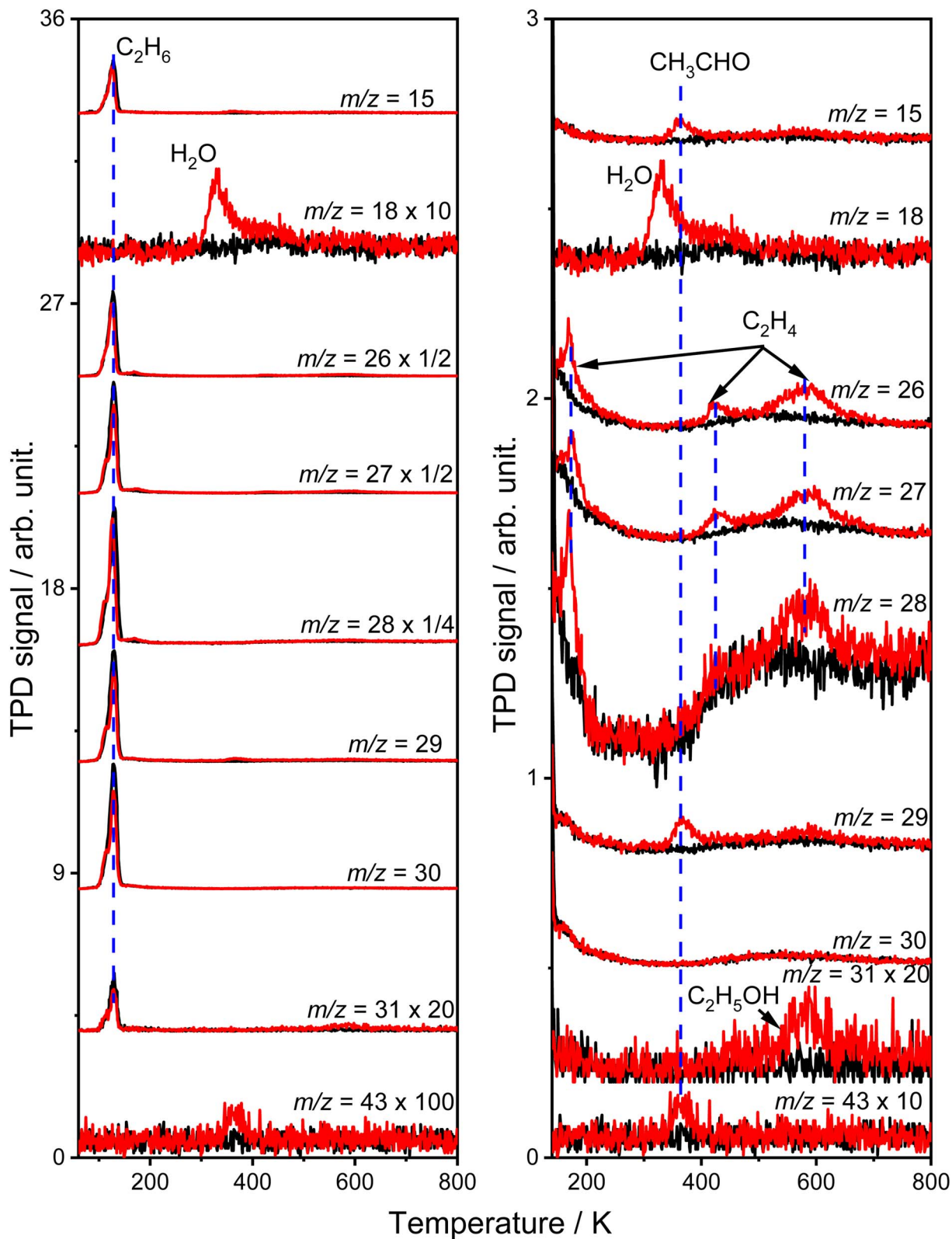


Fig. 1 Left: Typical TPD spectra acquired at  $m/z = 15$  ( $\text{CH}_3^+$ ), 18 ( $\text{H}_2\text{O}^+$ ), 26 ( $\text{C}_2\text{H}_2^+$ ), 27 ( $\text{C}_2\text{H}_3^+$ ), 28 ( $\text{C}_2\text{H}_4^+$  and  $\text{CO}^+$ ), 29 ( $\text{C}_2\text{H}_5^+$  and  $\text{CHO}^+$ ), 30 ( $\text{C}_2\text{H}_6^+$ ), 31 ( $\text{CH}_2\text{OH}^+$ ), and 43 ( $\text{CH}_3\text{CO}^+$ ) after irradiating the 0.28 ML  $\text{C}_2\text{H}_6$  covered oxidized R- $\text{TiO}_2(110)$  surfaces for 0 min (black lines) and 10 min (red lines) by 355 nm at 75 K, respectively. Right: The TPD spectra at the temperature range  $>140$  K are highlighted. The oxidized R- $\text{TiO}_2(110)$  surfaces were prepared by exposing the reduced surfaces to 200 L of  $\text{O}_2$  at 300 K. The photon flux of 355 nm light was  $2.1 \times 10^{16}$  photons per  $\text{cm}^2$  per s.

10)) found in the NIST database. Therefore, all three peaks could be assigned to the  $\text{C}_2\text{H}_4$  product, illustrating that the photocatalytic ODHE process to produce  $\text{C}_2\text{H}_4$  could be realized on oxidized R- $\text{TiO}_2$ (110).

Although the structure of  $\text{C}_2\text{H}_6$  was simpler than that of  $\text{C}_3\text{H}_8$ , and the initial C-H bond activation process for these two molecules was nearly the same, the pathways for  $\text{C}_2\text{H}_4$  production from photocatalytic ODHE on oxidized R- $\text{TiO}_2$ (110) were more complicated than that of the photocatalytic ODHP.<sup>25</sup> For the photocatalytic ODHP on R- $\text{TiO}_2$ (110), the majority of the propylene ( $\text{C}_3\text{H}_6$ ) product can be formed efficiently under UV irradiation at 100 K. Only a tiny amount of the  $\text{C}_3\text{H}_6$  product is formed at 340 K *via* the thermal dehydrogenation of the  $\text{C}_3\text{H}_7^-$  groups on the  $\text{Ti}_{5c}$  sites ( $\text{C}_3\text{H}_7(\text{Ti})^-$ ), whereas, no oxygenated carbon products were produced.<sup>25</sup> However, for methane ( $\text{CH}_4$ ) dehydrogenation *via* either thermocatalysis or photocatalysis,<sup>20,33</sup> the  $\text{CH}_3^+$  radicals are thought to be suspended above the  $\text{TiO}_2$  surface or to enter directly into the gas phase, showing a very high mobility. Therefore, once the  $\text{C}_2\text{H}_5^+$  radical is produced *via* photocatalytic ODHE on R- $\text{TiO}_2$ (110), it may also migrate on the surface or enter directly into the gas phase, in a similar way to the  $\text{CH}_3^+$  radical from  $\text{CH}_4$  conversion,<sup>20,33</sup> leading to the complicated reaction pathways in the photocatalytic ODHE process.

### Evidence of $\text{C}_2\text{H}_5^+$ radical formation and the fate of $\text{C}_2\text{H}_5^+$ radical

To confirm the formation of the  $\text{C}_2\text{H}_5^+$  radical intermediate in photocatalytic ODHE on R- $\text{TiO}_2$ (110), the PSD signals were collected at  $m/z = 26, 27, 28, 29$ , and 30 from the 0.28 ML  $\text{C}_2\text{H}_6$  covered oxidized R- $\text{TiO}_2$ (110) surface during the UV irradiation (Fig. 2). Upon irradiation, no obvious PSD signal was detected at  $m/z = 30$ , indicating that no photodesorption of  $\text{C}_2\text{H}_6$  had occurred. Conversely, sharp increases of the desorption signals at  $m/z = 26, 27$  and 28 were detected immediately when the UV light was on. The relative intensity of the PSD signals at  $m/z = 26$  and 27 was 0.89 : 1, suggesting that the signals were contributed by photo-desorbed  $\text{C}_2\text{H}_4$  molecules. In addition, a tiny PSD signal also appeared at  $m/z = 29$ , which may come from two sources. The first was due to the fragmentation of the  $\text{C}_2\text{H}_4$  product at  $m/z = 29$  (Fig. S4, ESI†). The other one was the  $\text{C}_2\text{H}_5^+$  radical product. However, due to the small PSD signal at  $m/z = 29$ , it was hard to determine whether a  $\text{C}_2\text{H}_5^+$  radical was formed.

Subsequently, the TOF method, which can enhance the detection sensitivity significantly by improving the SNR,<sup>34</sup> was used to monitor the desorbed products from the photocatalytic ODHE on R- $\text{TiO}_2$ (110) during the irradiation. As shown in Fig. 3, the TOF signals at  $m/z = 27$  ( $\text{C}_2\text{H}_3^+$ ), 29 ( $\text{C}_2\text{H}_5^+$ ) and 30 ( $\text{C}_2\text{H}_6^+$ ) were collected. Obvious peaks appeared in the TOF spectra of  $m/z = 27$  and 29. According to the result shown in Fig. 2, the TOF peak at  $m/z = 27$  was due to the desorption of  $\text{C}_2\text{H}_4$ . Interestingly, the relative intensities of the TOF signal at  $m/z = 27$  and 29 were about 3 : 1, which was much smaller than that of the  $\text{C}_2\text{H}_4$  sample (Fig. S4, ESI†). However, no discernible TOF signal at  $m/z = 30$  suggested that no photodesorption of  $\text{C}_2\text{H}_6$  had occurred, and this was consistent with the results in Fig. 2. As

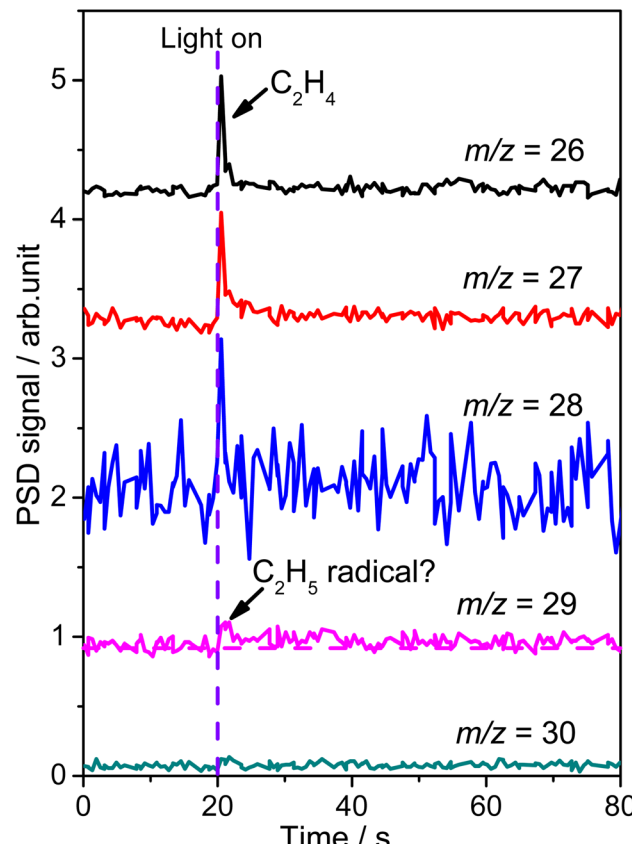
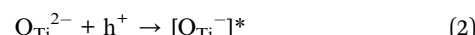
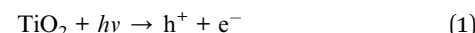


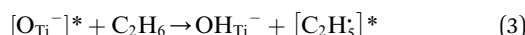
Fig. 2 The PSD spectra acquired at  $m/z = 26$  ( $\text{C}_2\text{H}_2^+$ ), 27 ( $\text{C}_2\text{H}_3^+$ ), 28 ( $\text{C}_2\text{H}_4^+$ ), 29 ( $\text{C}_2\text{H}_5^+$ ) and 30 ( $\text{C}_2\text{H}_6^+$ ) on the 0.28 ML  $\text{C}_2\text{H}_6$  covered oxidized R- $\text{TiO}_2$ (110) surfaces. The purple dashed line represents the moment when the light is turned on ( $t = 20$  s). The photon flux of the 355 nm light is  $2.4 \times 10^{16}$  photons per  $\text{cm}^2$  per s.

a result, the large TOF signal at  $m/z = 29$  could only be from the desorption of  $\text{C}_2\text{H}_5^+$  radical upon irradiation, illustrating that the initial photocatalytic C-H activation of  $\text{C}_2\text{H}_6$  on R- $\text{TiO}_2$ (110) produced the  $\text{C}_2\text{H}_5^+$  radical.

Thus, after the  $\text{O}_{\text{Ti}}^{2-}$  centers trap the photogenerated holes to form excited  $\text{O}_{\text{Ti}}^-$  centers:



the separated electrons are left on the R- $\text{TiO}_2$ (110). Then, because the  $\text{C}_2\text{H}_6$  was only weakly adsorbed on the surface, the direct hole transfer from R- $\text{TiO}_2$ (110) to  $\text{C}_2\text{H}_6$  was nearly impossible, and the reaction was most likely to occur *via* the abstraction of H atoms from  $\text{C}_2\text{H}_6$  by excited  $\text{O}_{\text{Ti}}^-$  centers to produce the  $\text{C}_2\text{H}_5^+$  radical:



When the  $\text{C}_2\text{H}_5^+$  radical was produced, it may further dehydrogenate spontaneously into  $\text{C}_2\text{H}_4$  and H atoms on the  $\text{O}_{\text{Ti}}^{2-}/\text{O}_\text{b}^{2-}$  sites or be ejected into the gas phase:<sup>21</sup>



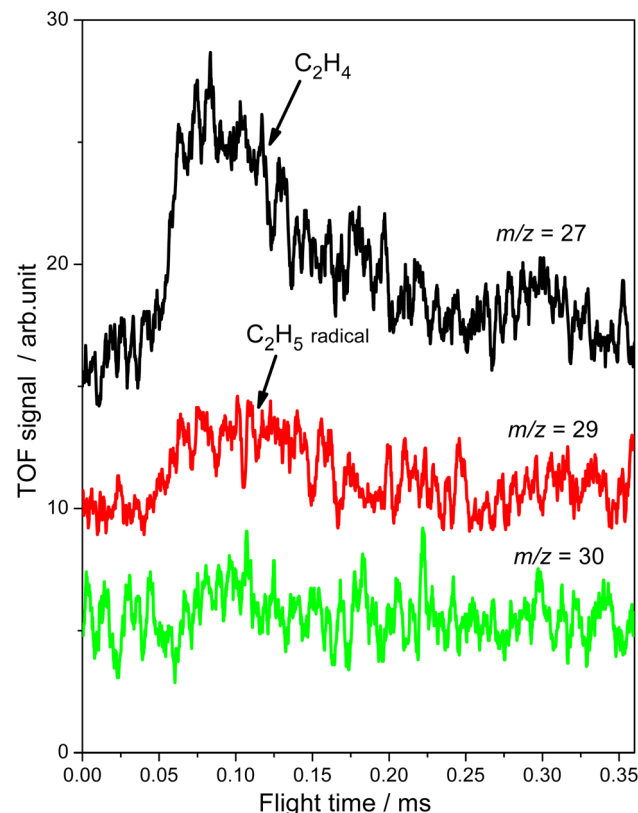
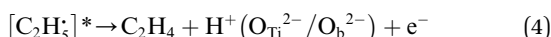


Fig. 3 The TOF signals of  $C_2H_4$  collected at  $m/z = 27$  ( $C_2H_3^+$ ), 29 ( $C_2H_5^+$ ) and 30 ( $C_2H_6^+$ ) as a function of the flight time when irradiating the 0.28 ML  $C_2H_6$  covered oxidized R-TiO<sub>2</sub>(110) surfaces at 343 nm. The photon flux of the 343 nm light is  $2.0 \times 10^{16}$  photons per  $cm^2$  per s.

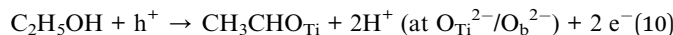
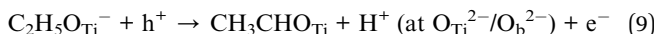


Here, it is not certain whether the second C–H bond cleavage needs another hole. The detection of the  $C_2H_5^*$  radical demonstrates that the interaction between the  $C_2H_5^*$  radical and the R-TiO<sub>2</sub>(110) was very weak. Therefore, the migration of the  $C_2H_5^*$  radical on the surface may occur easily. Once the  $C_2H_5^*$  radicals migrate on the surface, the  $C_2H_5^{(Ti)}^-$  groups, ethoxy groups ( $C_2H_5O_b^-$  and  $C_2H_5O_{Ti}^-$ ) and  $C_2H_5OH_{Ti}$  may be produced *via* the rebounding of the  $C_2H_5^*$  radicals to the  $Ti_{5c}$ ,  $O_b^{2-}$ ,  $O_{Ti}^{2-}$  and  $OH_{Ti}^-$  groups:<sup>35</sup>



Among them, the  $C_2H_5^{(Ti)}^-$  groups would further dehydrogenate into  $C_2H_4$  *via* a similar thermocatalytic pathway used for the thermocatalytic  $C_3H_6$  formation,<sup>25</sup> giving a  $C_2H_4$  desorption

peak at 423 K. The  $C_2H_5O_{Ti}^-/C_2H_5OH_{Ti}$  will decompose into  $CH_3CHO_{Ti}$  easily upon irradiation:<sup>36,37</sup>



During the reaction steps, most of the steps were hole induced half-reactions, which will leave electrons on the surface. It seems that the photocatalytic ODHE on R-TiO<sub>2</sub>(110) will produce excess electrons on the surface. In fact, when the reduced R-TiO<sub>2</sub>(110) surface is oxidized by  $O_2$  at room temperature to form the  $O_{Ti}$  covered surface, the surface  $O_b$  vacancies will be healed, the excess electrons of R-TiO<sub>2</sub>(110) contributed by the vacancies ( $O_v^{2-}$ ) and Ti interstitials ( $Ti^{3+}$ ) under the surface or in the bulk, will be trapped by the dissociated  $O_{Ti}$  atoms to form  $O_{Ti}^{2-}$ .<sup>25,27,28</sup> Upon irradiation, after the electron–hole separation, the holes will be trapped at the  $O_b^{2-}$  and  $O_{Ti}^{2-}$ , forming  $O_b^-$  and  $O_{Ti}^-$ . The photogenerated electrons will be trapped by the vacancies and Ti interstitials that gave the electrons to the surface of the  $O_{Ti}$  atoms before. Similarly, in the later reactions, even electrons are left behind, and most of them are probably trapped by vacancies and the Ti interstitials. As a result, although the excess electrons of R-TiO<sub>2</sub>(110) did not transfer to  $C_2H_6$  and  $C_2H_5O_{Ti}^-/C_2H_5OH_{Ti}$  during the photocatalytic ODHE process, they are trapped by  $O_{Ti}$  atoms initially to form  $O_{Ti}^{2-}$ , and most of them go back to the surface after the reactions because the formation of low temperature  $C_2H_4$  and  $CH_3CHO$  are whole reactions, not half reactions. The overall reaction *via* photocatalysis follows eqn (11):



In addition, the minor reaction pathways of reactions in eqn (5) and (6) may produce excess electrons on the surface.

Furthermore, although the  $C_2H_5O_b^-$  groups have little photo reactivity,<sup>36</sup> the  $C_2H_5O_b^-$  groups could dissociate to  $C_2H_4$  with a small amount of  $C_2H_5OH$  product during the TPD process,<sup>38</sup> which was consistent with our TPD result for the  $C_2H_5OH$  desorption on the  $O_v$  sites of R-TiO<sub>2</sub>(110) (Fig. S5, ESI†). Therefore, the  $C_2H_4$  formation at 580 K was due to the thermocatalytic dehydrogenation of the  $C_2H_5O_b^-$  groups, and the tiny peak at 585 K ( $m/z = 31$ ) may be assigned to the recombinational  $C_2H_5OH$  desorption from the  $C_2H_5O_b^-$  groups and dissociated protons ( $H^+$ ) during the TPD process.

To evaluate the importance of the  $C_2H_4$  production *via* photocatalytic ODHE on R-TiO<sub>2</sub>(110), the formation of carbon containing products and  $H_2O$  were monitored using the TPD traces of  $m/z = 18$ , 27, 29, and 31 collected on the 0.28 ML  $C_2H_6$  covered oxidized R-TiO<sub>2</sub>(110) surfaces as a function of irradiation time (Fig. 4). As the irradiation time increased, the signals of the thermocatalytic products (the 423 K ( $C_2H_4$ ), 580 K ( $C_2H_4$ ), and 585 K ( $C_2H_5OH$ ) peaks) increased very fast and reached plateaus after approximately 60 s irradiation (the green traces). However, the signals of the 168 K ( $C_2H_4$ ), 330 K ( $H_2O$ ), and 365 K peaks ( $CH_3CHO$ ) increased slowly and almost reached plateaus after 600 s irradiation. As discussed, previously, the  $O_{Ti}$  is



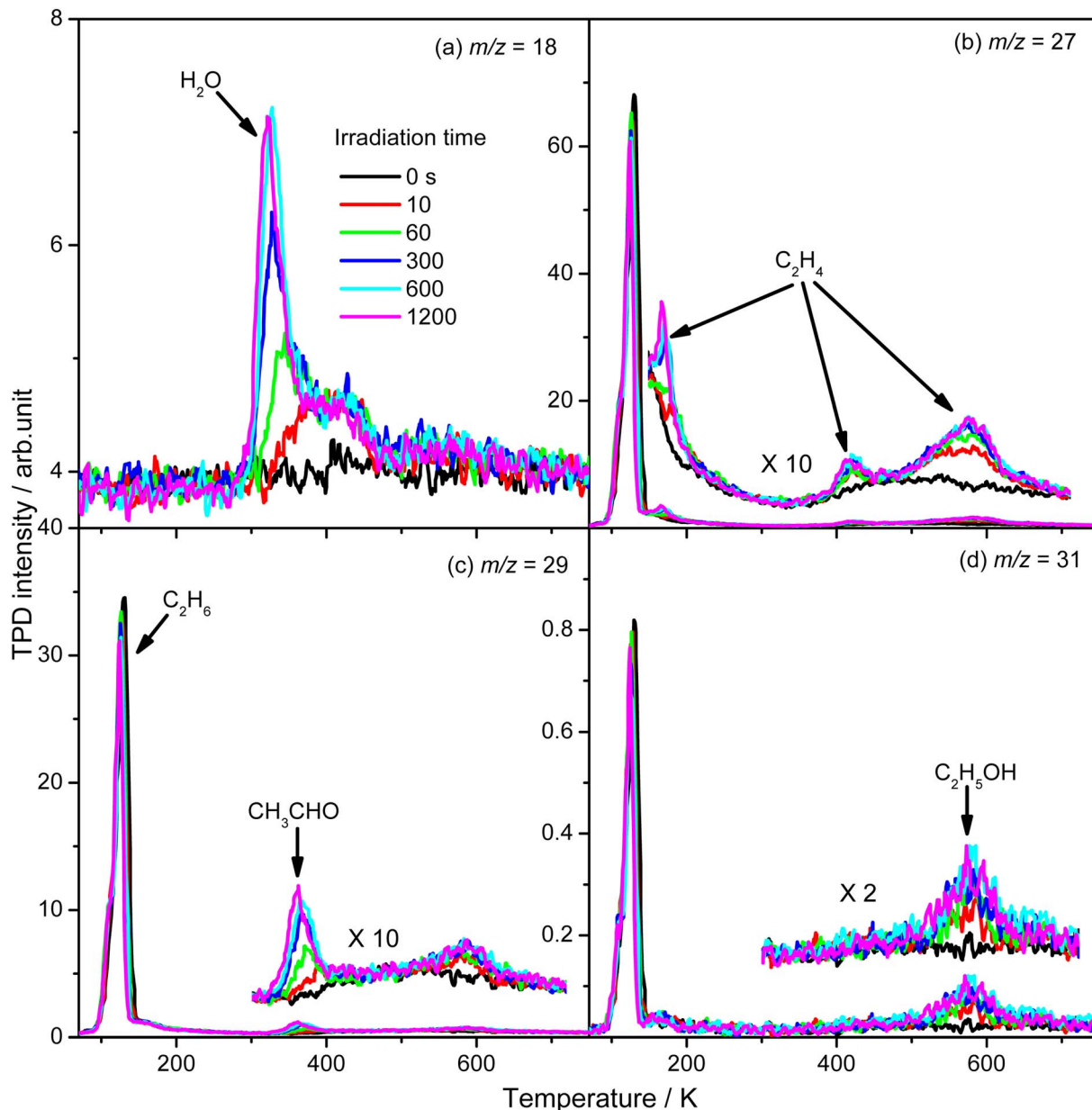


Fig. 4 The TPD spectra acquired at  $m/z = 18$  ( $\text{H}_2\text{O}^+$ ) (a),  $27$  ( $\text{C}_2\text{H}_3^+$ ) (b),  $29$  ( $\text{C}_2\text{H}_5^+$ ) (c), and  $31$  ( $\text{CH}_3\text{O}^+$ ) (d) on the  $0.28$  ML  $\text{C}_2\text{H}_6$  covered oxidized  $\text{R-TiO}_2(110)$  surfaces as a function of irradiation time. The desorption peaks of the carbon containing products are highlighted in the inserts of (b-d).

involved in the formation of  $168$  K ( $\text{C}_2\text{H}_4$ ),  $330$  K ( $\text{H}_2\text{O}$ ), and  $365$  K ( $\text{CH}_3\text{CHO}$ ) products. Here, the coverage of  $\text{O}_{\text{Ti}}$  atoms on the surface was only about  $0.06$ – $0.07$  ML, which was strongly dependent on the concentration of the  $\text{O}_v$  sites.<sup>27,28</sup> In contrast, the coverages of  $\text{Ti}_{5c}$  and  $\text{O}_b$  sites on the oxidized  $\text{R-TiO}_2(110)$  were nearly  $1.0$  ML. As a result, the possibility for the  $\text{C}_2\text{H}_5$  moieties bonding to the  $\text{Ti}_{5c}$  and  $\text{O}_b$  sites to produce  $\text{C}_2\text{H}_5\text{O}_{\text{Ti}}^-$  and  $\text{C}_2\text{H}_5\text{O}_b^-$  groups would be much higher than that for the  $\text{C}_2\text{H}_5$  moieties bonding to  $\text{O}_{\text{Ti}}^{2-}/\text{OH}_{\text{Ti}}^-$  to produce  $\text{C}_2\text{H}_5\text{O}_{\text{Ti}}^-/\text{C}_2\text{H}_5\text{OH}_{\text{Ti}}$ , resulting in the formation of  $\text{C}_2\text{H}_5\text{O}_{\text{Ti}}^-$  and  $\text{C}_2\text{H}_5\text{O}_b^-$  groups much faster than the  $\text{C}_2\text{H}_5\text{O}_{\text{Ti}}^-/\text{C}_2\text{H}_5\text{OH}_{\text{Ti}}$ .

From Fig. 4, the yields of  $\text{H}_2\text{O}$  and carbon containing products ( $\text{C}_2\text{H}_4$ ,  $\text{CH}_3\text{CHO}$ , and  $\text{C}_2\text{H}_5\text{OH}$ ) were derived and are plotted in Fig. 5. The total yield of  $\text{C}_2\text{H}_4$  contained the  $168$  K,  $423$  K, and  $580$  K peaks. With an increasing irradiation time, the difference between the yield of  $\text{H}_2\text{O}$  and carbon containing products became larger and larger. At  $20$  min irradiation, about  $0.041$  ML of  $\text{H}_2\text{O}$  was produced, and the yields of  $\text{C}_2\text{H}_5\text{OH}$ ,  $\text{CH}_3\text{CHO}$ , and  $\text{C}_2\text{H}_4$  are about  $0.004$  ML,  $0.0075$  ML, and  $0.02$  ML, respectively. Combining the results from Fig. 2 and 3, it was seen that the big difference between the yields of  $\text{H}_2\text{O}$  and carbon containing products was due to the photo-desorbed  $\text{C}_2\text{H}_4$  and  $\text{C}_2\text{H}_5$  radicals. Therefore, the  $\text{C}_2\text{H}_4$  product

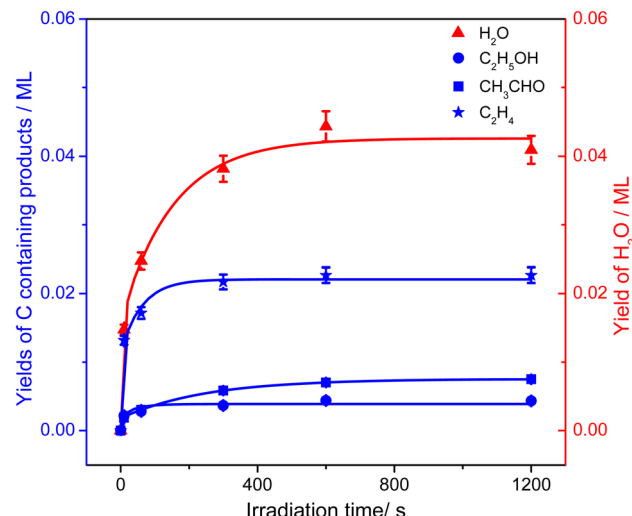


Fig. 5 The yields of  $\text{H}_2\text{O}$  (red triangles) and carbon containing products ( $\text{C}_2\text{H}_5\text{OH}$  (blue circles),  $\text{CH}_3\text{CHO}$  (blue squares), and  $\text{C}_2\text{H}_4$  (blue stars)) in photocatalytic ODHE on oxidized  $\text{R-TiO}_2(110)$  as a function of irradiation time, derived from Fig. 4. All the plotted lines are only to guide the eye.

(including the 168 K, 423 K, and 580 K peaks) was the main product in photocatalytic ODHE on  $\text{R-TiO}_2(110)$ .

### Microscopic kinetics of the $\text{C}_2\text{H}_4$ formation

Similar to the case of the other hydrocarbons ( $\text{C}_3\text{H}_8$ , ethylbenzene ( $\text{C}_6\text{H}_5\text{C}_2\text{H}_5$ , EB)),<sup>25,39</sup> the initial C–H bond activation of  $\text{C}_2\text{H}_6$  could be induced by hole trapped  $\text{O}_{\text{Ti}}^-$ . However, the second C–H bond cleavage in the  $\text{C}_2\text{H}_6$  conversion on  $\text{R-TiO}_2(110)$  was still not clear. On the one hand, the  $\text{C}_2\text{H}_5$  radicals may further dehydrogenate into  $\text{C}_2\text{H}_4$  directly,<sup>21</sup> suggesting that the whole process only needs one hole. On the other hand, because the  $\text{C}_2\text{H}_5$  radicals can decay into  $\text{C}_2\text{H}_{5(\text{Ti})}^-$  groups *via* the de-excitation process, the  $\text{C}_2\text{H}_{5(\text{Ti})}^-$  group may also trap another hole to form a  $\text{C}_2\text{H}_5$  radical again for  $\text{C}_2\text{H}_4$  production. For this process, a total of two holes are consumed for the stepwise  $\text{C}_2\text{H}_4$  production. Although the involvement of  $\text{C}_2\text{H}_{5(\text{Ti})}^-$  in photocatalytic ODHE does not affect  $\text{C}_2\text{H}_4$  production macroscopically, the microkinetic mechanism is very distinct.

To confirm whether  $\text{C}_2\text{H}_{5(\text{Ti})}^-$  is involved in photocatalytic ODHE into  $\text{C}_2\text{H}_4$  on  $\text{R-TiO}_2(110)$ , the PSD signals of  $\text{C}_2\text{H}_4$  at  $m/z = 27$  were collected from the 0.28 ML  $\text{C}_2\text{H}_6$  covered oxidized  $\text{R-TiO}_2(110)$  surfaces as a function of the laser power. As the laser power increased, the intensity of the  $\text{C}_2\text{H}_4$  PSD signal (the initial data point in each photodesorption experiment) increased significantly. More importantly, the intensity of the PSD signal of the  $\text{C}_2\text{H}_4$  scaled linearly with the square root of the photon flux ( $F_{h\nu}^{1/2}$ ) (see the inset of Fig. 6). According to the results of previous work on  $\text{O}_2$  photodesorption on  $\text{R-TiO}_2(110)$ <sup>40,41</sup> and  $\text{C}_2\text{H}_5\text{OH}$  photodecomposition on  $\text{R-TiO}_2(110)$ ,<sup>42</sup> such a linear relationship illustrates that the photocatalytic ODHE to  $\text{C}_2\text{H}_4$  on oxidized  $\text{R-TiO}_2(110)$  was governed by the second-order electron–hole ( $\text{h}^+/\text{e}^-$ ) pair recombination kinetics, and only one

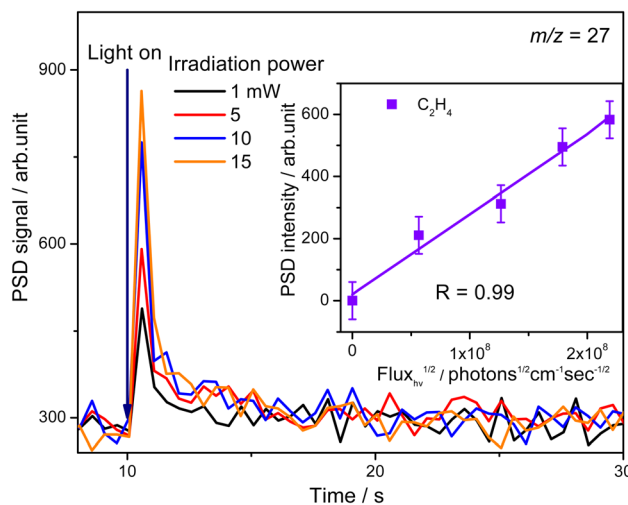


Fig. 6 The PSD signals of  $\text{C}_2\text{H}_4$  collected from the 0.28 ML  $\text{C}_2\text{H}_6$  covered oxidized  $\text{R-TiO}_2(110)$  surfaces as a function of the laser irradiation power. The intensity of the PSD signals (the initial point when the UV light is turned on) of  $\text{C}_2\text{H}_4$  has a linear relationship with the square root of the incident light flux ( $F_{h\nu}^{1/2}$ ), as shown in the inset of this figure.

hole (or one photon) was involved in the complicated process. Furthermore, the pathway of  $\text{C}_2\text{H}_4$  production from the photocatalytic ODHE on oxidized  $\text{R-TiO}_2(110)$  with the involvement of  $\text{C}_2\text{H}_{5(\text{Ti})}^-$  could be ruled out, because it needs two holes (or photons). Therefore, the  $\text{C}_2\text{H}_4$  formation from photocatalytic ODHE on oxidized  $\text{R-TiO}_2(110)$  occurs in a stepwise manner, in which the  $\text{C}_2\text{H}_6$  first undergoes the initial C–H bond cleavage to form  $\text{C}_2\text{H}_5$  radicals with the help of hole trapped  $\text{O}_{\text{Ti}}^-$  centers, and is then followed by further spontaneous dehydrogenation of the  $\text{C}_2\text{H}_5$  radicals into  $\text{C}_2\text{H}_4$  without the involvement of an extra photon or hole. During the  $\text{C}_2\text{H}_4$  formation process, the initial C–H bond activation is the rate-limiting step.

In addition, as shown in Fig. S6 (ESI),<sup>†</sup>  $\text{C}_2\text{H}_4$  can be photodesorbed on the  $\text{C}_2\text{H}_4$  covered  $\text{R-TiO}_2(110)$ , indicating that the desorption of  $\text{C}_2\text{H}_4$  was induced by the photogenerated charge carriers (electron or hole). If the  $\text{C}_2\text{H}_4$  product from the photocatalytic ODHE prefers to adsorb on the  $\text{R-TiO}_2(110)$  surface first, and then be photo-desorbed from the surface, at least two photons are consumed for the  $\text{C}_2\text{H}_4$  formation and desorption processes. However, the whole process was accomplished by one hole (or one photon), thus, once  $\text{C}_2\text{H}_4$  was formed by further C–H bond cleavage of the  $\text{C}_2\text{H}_5$  radicals, it was preferentially ejected directly into the vacuum rather than being adsorbed on the surface followed by photoinduced desorption. Therefore, only a tiny signal for the  $\text{C}_2\text{H}_{4(\text{Ti})}$  desorption can be observed during the TPD process.

### Discussion

As shown previously, both reduced and oxidized  $\text{R-TiO}_2(110)$  surfaces do not show thermocatalytic reactivities for  $\text{C}_2\text{H}_6$  activation. This was very different from the results of the C–H activation of the light alkanes on the  $\text{PdO}(101)$ ,  $\text{RuO}_2(110)$ , and  $\text{IrO}_2(110)$  surfaces,<sup>43–46</sup> in which alkanes adsorb on these



surfaces stably by forming strongly adsorbed  $\sigma$ -complex species as the precursor, leading to a weakening of the C–H bond in the alkanes. Similarly, Yue and co-workers proposed that the initial C–H bond activation of  $\text{C}_2\text{H}_6$  on the M/TiO<sub>2</sub> (M = Pd and Cu) surfaces was realized *via* the interaction of  $\text{C}_2\text{H}_6$  with the surface sites to produce surface  $\text{C}_2\text{H}_5^-$  groups, and then the  $\text{C}_2\text{H}_5^-$  groups trapped the photogenerated holes to form  $\text{C}_2\text{H}_5^\cdot$  radicals, which converted rapidly into the  $\text{C}_2\text{H}_4$  product.<sup>22,24</sup> However, although the R-TiO<sub>2</sub>(110) has the same surface structure with RuO<sub>2</sub>(110) and IrO<sub>2</sub>(110), the weak interaction between the  $\text{C}_2\text{H}_6$  and Ti<sub>5c</sub> sites of R-TiO<sub>2</sub>(110) inhibit the formation of the  $\text{C}_2\text{H}_6$   $\sigma$ -complex. As a result, the H atom abstraction from  $\text{C}_2\text{H}_6$  by the O<sub>b</sub> and O<sub>Ti</sub> atoms (or O<sub>b</sub><sup>2-</sup> and O<sub>Ti</sub><sup>2-</sup>) following the Langmuir–Hinshelwood (L–H) mechanism is difficult. Namely, the initial C–H bond activation of  $\text{C}_2\text{H}_6$  on R-TiO<sub>2</sub>(110) seems to occur ineffectively at the ground state *via* thermocatalysis.<sup>21,22,24</sup>

However, when the O<sub>b</sub><sup>2-</sup> and O<sub>Ti</sub><sup>2-</sup> centers trap photogenerated holes, the nucleophilic O<sub>b</sub><sup>2-</sup> and O<sub>Ti</sub><sup>2-</sup> convert into electrophilic O<sub>b</sub><sup>-</sup> and O<sub>Ti</sub><sup>-</sup> centers,<sup>47,48</sup> which have a stronger ability than O<sub>b</sub><sup>2-</sup> and O<sub>Ti</sub><sup>2-</sup> to abstract the H atoms of the small alkanes.<sup>20,21,25</sup> Correspondingly, the study of the photocatalytic EB dehydrogenation on R-TiO<sub>2</sub>(110)<sup>39</sup> demonstrated that both the O<sub>b</sub><sup>-</sup> and O<sub>Ti</sub><sup>-</sup> centers produced by trapping the holes can activate the  $\alpha$ -C–H bond of the side chain alkyl groups of EB. In addition, theoretical works also suggest that the O<sub>b</sub><sup>-</sup> centers formed upon the UV irradiation play a vital role in the C–H bond activation of CH<sub>4</sub> and  $\text{C}_2\text{H}_6$  on R-TiO<sub>2</sub>(110).<sup>20,21</sup> Unfortunately, no product signal of photocatalytic ODHE was detected on reduced R-TiO<sub>2</sub>(110) (Fig. S1, ESI<sup>†</sup>) under 355 nm irradiation, indicating that the O<sub>b</sub><sup>-</sup> center produced with the 355 nm irradiation finds it difficult to activate the inert C–H bond of  $\text{C}_2\text{H}_6$  under the current conditions.

In contrast, the EB can be regarded as one H atom of the  $\text{C}_2\text{H}_6$  molecule substituted by a phenyl group (C<sub>6</sub>H<sub>5</sub>), in which the C–H bond of the ethyl group can be activated efficiently by the hole-trapped O<sub>b</sub><sup>-</sup> center.<sup>39</sup> The difference in the initial C–H bond activation of  $\text{C}_2\text{H}_6$  and EB by the O<sub>b</sub><sup>-</sup> center on R-TiO<sub>2</sub>(110) may be because of two possible reasons. Firstly, compared with the H atom, the phenyl group as an electron withdrawing group will decrease the electron density of the  $\alpha$ -C in the  $\text{C}_2\text{H}_5$  group *via* a  $\sigma$ – $\pi$  hyperconjugation, resulting in weakening of the  $\alpha$ -C–H bond. As a result, the  $\alpha$ -C–H bond will be activated more easily than the C–H bond of  $\text{C}_2\text{H}_6$ . Secondly, the desorption temperature of EB on R-TiO<sub>2</sub>(110)<sup>39</sup> was much higher than that of  $\text{C}_2\text{H}_6$  by about 120 K, indicating that the former has a stronger interaction between the aromatic ring and the surface, which may be more beneficial for energy and charge transfer between adsorbates with the surface, leading to the second C–H bond cleavage of EB.

In addition, for C<sub>3</sub>H<sub>8</sub>, one H atom of the  $\text{C}_2\text{H}_6$  molecule substituted by a methyl group (CH<sub>3</sub><sup>-</sup>), contained two types of C–H bonds (1° and 2°), and its structure was more complicated than that of  $\text{C}_2\text{H}_6$ . However, the C<sub>3</sub>H<sub>8</sub> was produced with a high selectivity *via* photocatalytic ODHP on R-TiO<sub>2</sub>(110), and no oxygenates were produced,<sup>25</sup> indicating that the reaction intermediates in the photocatalytic ODHP did not show high

mobility on the surface. This was most likely due to the different interaction strengths between different intermediates with R-TiO<sub>2</sub>(110). According to the desorption temperature of C<sub>2</sub>H<sub>6</sub> (Fig. 1) and C<sub>3</sub>H<sub>8</sub>,<sup>25,29</sup> both C<sub>2</sub>H<sub>6</sub> and C<sub>3</sub>H<sub>8</sub> were weakly bound to the surface, causing both C<sub>2</sub>H<sub>6</sub> and C<sub>3</sub>H<sub>8</sub> to easily migrate on the surface. As a result, the initial C–H bond activation of  $\text{C}_2\text{H}_6$  on R-TiO<sub>2</sub>(110) was more likely to follow the O<sub>Ti</sub> atom mediated Eley–Rideal (E–R) mechanism,<sup>1,25</sup> forming a movable  $\text{C}_2\text{H}_5^\cdot$  radical by the abstraction of an H atom from  $\text{C}_2\text{H}_6$  by an excited O<sub>Ti</sub><sup>-</sup> center, which may significantly affect the selectivity of the products. The interaction between the  $\text{C}_2\text{H}_5^\cdot$  radicals, which were worse electron donors, with the Ti<sub>5c</sub> sites should be weaker than that of the possible C<sub>3</sub>H<sub>7</sub><sup>·</sup> radicals produced in the photocatalytic ODHP on R-TiO<sub>2</sub>(110), which tended to form an allyl  $\sigma$ –p hyperconjugation configuration (CH<sub>3</sub>CH'CH<sub>3</sub>) with a stronger electron-donating ability.<sup>25,49</sup> Then, the  $\text{C}_2\text{H}_5^\cdot$  radicals may migrate on the surface more easily, resulting in the formation of additional byproducts *via* the diffusion and rebounding processes.

Similarly, previous research on the photooxidation of *tert*-butanol and ketones on R-TiO<sub>2</sub>(110) also observed C<sub>2</sub>H<sub>5</sub><sup>·</sup> radical ejection,<sup>50–52</sup> which was associated with hole-induced chemistry.<sup>20,21,25,50,52</sup> According to the work on CH<sub>3</sub><sup>·</sup> radical formation from ketone photooxidation on R-TiO<sub>2</sub>(110),<sup>52</sup> two dissociation channels (“fast” and “slow” channels) of the CH<sub>3</sub><sup>·</sup> radical desorption were detected. The “fast” CH<sub>3</sub><sup>·</sup> radical production was attributed to the prompt dissociation of an internally “hot” acetone–oxygen complex (intermediates at the excited state), and the acetone–oxygen complex weakly coupled to the surface. However, the “slow” CH<sub>3</sub><sup>·</sup> radical production was assigned to the dissociation of a relaxed acetone–oxygen complex formed *via* internal vibrational redistribution (IVR), which consumed the available energy for the C–C bond cleavage. In the case of the C<sub>2</sub>H<sub>5</sub><sup>·</sup> radical ejection from 2-butanone photooxidation on R-TiO<sub>2</sub>(110), the “slow” channel dominated.<sup>50</sup> As a result, no obvious C<sub>2</sub>H<sub>4</sub> product obtained from C<sub>2</sub>H<sub>5</sub><sup>·</sup> radical dehydrogenation was detected.<sup>50</sup>

However, for the photocatalytic ODHE on the R-TiO<sub>2</sub>(110) surface, C<sub>2</sub>H<sub>6</sub> was also weakly adsorbed on the surface and its structure was very simple without a  $\pi$ -conjugated system, and the IVR process will not occur to make the “hot” C<sub>2</sub>H<sub>5</sub><sup>·</sup> radical relax efficiently, thus resulting in the further dehydrogenation of the excited C<sub>2</sub>H<sub>5</sub><sup>·</sup> radical into C<sub>2</sub>H<sub>4</sub>. Compared with these results,<sup>50–52</sup> it was not too difficult to conclude that the IVR process can affect the energy relaxation in excited molecules or ions on the R-TiO<sub>2</sub>(110) surface, which can further affect the bond breaking and product formation. The smaller molecules (such as C<sub>2</sub>H<sub>6</sub>) may inhibit the IVR process in photocatalytic reactions due to having fewer vibrational energy levels than complicated molecules, leading to the high efficiency of bond breaking.

Due to the formation of weakly bonded C<sub>2</sub>H<sub>5</sub><sup>·</sup> radical intermediates, it is reasonable that oxygen-containing species are formed *via* the rebounding between the C<sub>2</sub>H<sub>5</sub><sup>·</sup> radicals and the surface O atoms (O<sub>b</sub><sup>2-</sup> and O<sub>Ti</sub><sup>2-</sup>). However, based on previous research about ODHE over vanadium oxides,<sup>53–55</sup> terminal M=O species (terminal metal oxo, V=O) are the active sites for



ODHE, in which either the direct insertion of the C–H bond across the M=O bond resulted in  $\text{C}_2\text{H}_5\text{O}$  group formation or C–H bond activation by H abstraction to form M–OH and a transient alkyl radical product ( $\text{C}_2\text{H}_5^\bullet$ ) may occur. If the  $\text{C}_2\text{H}_5\text{O}_\text{b}^-$  formation occurs *via* the  $\text{O}_\text{b}^{2-}$  insertion pathway, the  $\text{C}_2\text{H}_4$  product formed at 580 K by the dehydrogenation of  $\text{C}_2\text{H}_5\text{O}_\text{b}^-$  groups should be observed on both the reduced and oxidized R-TiO<sub>2</sub>(110) surfaces. However, the formation of the  $\text{C}_2\text{H}_5\text{O}_\text{b}^-$  groups was only detected on the oxidized surface, suggesting that the  $\text{C}_2\text{H}_5\text{O}_\text{b}^-$  groups were produced *via* the recombination of the  $\text{C}_2\text{H}_5^\bullet$  radical and  $\text{O}_\text{b}^{2-}$  rather than the  $\text{O}_\text{b}^{2-}$  insertion pathway. In addition, the direct insertion generally has a high barrier,<sup>54,55</sup> which is difficult for  $\text{C}_2\text{H}_6$  activation on TiO<sub>2</sub> following the L–H mechanism due to weak adsorption energy. Despite all this, the existence of a direct heterolytic insertion of  $\text{O}_\text{Ti}^-$  to  $\text{C}_2\text{H}_6$  for  $\text{C}_2\text{H}_5\text{O}_\text{Ti}^-/\text{C}_2\text{H}_5\text{OH}_\text{Ti}$  formation cannot be completely ruled out.

Interestingly, although the initial C–H bond cleavage of EB on R-TiO<sub>2</sub>(110) occurred more easily than that of  $\text{C}_2\text{H}_6$ , the possible radical intermediate ( $\text{C}_8\text{H}_9^\bullet$ ) produced from the initial C–H bond cleavage of EB under UV irradiation preferred to decay to  $\text{C}_8\text{H}_9^-$  rather than further dehydrogenate into styrene directly, leading to a low yield of low temperature styrene production.<sup>39</sup> In contrast, in the case of  $\text{C}_2\text{H}_6$  and  $\text{C}_3\text{H}_8$  activation<sup>25</sup> on R-TiO<sub>2</sub>(110), the intermediates mainly dehydrogenated into  $\text{C}_2\text{H}_4$  and  $\text{C}_3\text{H}_6$  spontaneously, whereas only tiny radicals decay to alkyl groups adsorbed on the Ti<sub>5c</sub> sites. This suggested that the photon energy for the C–H bond activation of small alkanes into alkenes *via* TiO<sub>2</sub> photocatalysis may be utilized more efficiently than that of aromatic EB.<sup>39,56</sup> Furthermore, due to phenyl group substitution, the rate-determining step of the photocatalytic dehydrogenation of hydrocarbons into corresponding alkenes shifts from the initial C–H bond activation to the second further dehydrogenation.<sup>25,39</sup> This result may be more evidence that the IVR process in the larger molecule reduces the available energy for bond breaking. In order to overcome the consumption of available energy by the IVR process, excitation with higher energy photons may be a feasible way. Referring to the results of the recent photocatalytic conversion of EB into styrene on R-TiO<sub>2</sub>(100),<sup>56</sup> the efficiency of the initial  $\alpha$ -C–H bond activation is nearly the same at 257 nm and 343 nm, whereas the rate of the  $\beta$ -C–H bond cleavage was strongly enhanced with the photon energy. In contrast, for  $\text{C}_2\text{H}_6$  and  $\text{C}_3\text{H}_8$ ,<sup>21,25</sup> once the initial C–H bond cleavage was activated by the hole derived from the 355 nm photoexcitation with a lower photon energy, the second dehydrogenation was still accomplished quite easily. However, the mobility of the intermediates determined the complexity of the reactions.

## Conclusion

In summary, photocatalytic ODHE on the model R-TiO<sub>2</sub>(110) surface has been systematically investigated to determine the mechanism of the process. The  $\text{C}_2\text{H}_4$  formation for the photocatalytic ODHE on the oxidized surface can be achieved *via* a stepwise manner at 75 K, in which the  $\text{C}_2\text{H}_5^\bullet$  radical

intermediate is detected directly. The hole trapped  $\text{O}_\text{Ti}^-$  centers play a crucial role in the initial C–H bond activation of  $\text{C}_2\text{H}_6$ , and only one hole is involved in the cleavage of the two C–H bonds to produce  $\text{C}_2\text{H}_4$ . This result not only illustrates that photocatalysis is very suitable for the inert C–H bond activation of small alkanes, but also provides a novel mechanistic insight into photocatalytic ODHE, which offers new opportunities for the development of novel ODHE pathways with high  $\text{C}_2\text{H}_4$  selectivity under mild conditions.

## Data availability

The data supporting this study is available within the main text and the associated ESI.†

## Author contributions

YL and YZ conducted the TPD experiments and analysis. XC and TW helped to conduct the TPD experiments, and to revise the manuscript. FL and QG conceived the idea, designed the experiment, analyzed the data, and co-wrote the paper. XY supervised the research. All the authors discussed the results and commented on the paper.

## Conflicts of interest

The authors declare no competing financial interests.

## Acknowledgements

This work was supported by the National Key R&D Program of China (Grant No. 2022YFA1503102, 2018YFE0203002), the National Natural Science Foundation of China (NSFC Center for Chemical Dynamics, Grant No. 22173041, 22103033, 22103031, 22173042, 21973037), the Strategic Priority Research Program of Chinese Academy of Sciences (Grant No. XDB17000000), the Shenzhen Science and Technology Innovation Committee (Grant No. 20220814164755002, ZDSYS2020042111001787), the Guangdong Innovative & Entrepreneurial Research Team Program (Grant No. 2019ZT08L455, 2019JC01X091), the International Partnership Program of Chinese Academy of Sciences (Grant No. 121421KYSB20170012), and the Innovation Program for Quantum Science and Technology (Grant No. 2021ZD0303304).

## References

- 1 S. Najari, S. Saeidi, P. Concepcion, D. D. Dionysiou, S. K. Bhargava, A. F. Lee and K. Wilson, *Chem. Soc. Rev.*, 2021, **50**, 4564–4605.
- 2 Y. Dai, X. Gao, Q. Wang, X. Wan, C. Zhou and Y. Yang, *Chem. Soc. Rev.*, 2021, **50**, 5590–5630.
- 3 R. Gudgila and C. A. Leclerc, *Ind. Eng. Chem. Res.*, 2011, **50**, 8438–8443.
- 4 P. Sun, G. Siddiqi, W. C. Vining, M. Chi and A. T. Bell, *J. Catal.*, 2011, **282**, 165–174.



5 J.-P. Lange, R. Schoonebeek, P. Mercera and F. Van Breukelen, *Appl. Catal., A*, 2005, **283**, 243–253.

6 V. Zacharopoulou and A. A. Lemonidou, *Catalysts*, 2017, **8**, 2.

7 S. Najari, S. S. Hosseini, M. Omidkhah and N. R. Tan, *RSC Adv.*, 2015, **5**, 47199–47215.

8 A. Corma, E. Corresa, Y. Mathieu, L. Sauvanaud, S. Al-Bogami, M. Al-Ghrami and A. Bourane, *Catal. Sci. Technol.*, 2017, **7**, 12–46.

9 M. Sun, J. Zhang, P. Putaj, V. Caps, F. d. r. Lefebvre, J. Pelletier and J.-M. Basset, *Chem. Rev.*, 2014, **114**, 981–1019.

10 J. T. Grant, J. M. Venegas, W. P. McDermott and I. Hermans, *Chem. Rev.*, 2017, **118**, 2769–2815.

11 C. A. Gärtner, A. C. van Veen and J. A. Lercher, *ChemCatChem*, 2013, **5**, 3196–3217.

12 Y. Zhou, J. Lin, L. Li, X. Pan, X. Sun and X. Wang, *J. Catal.*, 2018, **365**, 14–23.

13 Y. Honda, A. Takagaki, R. Kikuchi and S. T. Oyama, *Chem. Lett.*, 2018, **47**, 1090–1093.

14 T.-K. Cheung and B. C. Gates, *J. Catal.*, 1997, **168**, 522–531.

15 S. Wang, K. Murata, T. Hayakawa, S. Hamakawa and K. Suzuki, *Chem. Commun.*, 1999, 103–104.

16 E. Gomez, B. Yan, S. Kattel and J. G. Chen, *Nat. Rev. Chem.*, 2019, **3**, 638–649.

17 S. Deng, S. Li, H. Li and Y. Zhang, *Ind. Eng. Chem. Res.*, 2009, **48**, 7561–7566.

18 S. Yusuf, L. Neal, V. Haribal, M. Baldwin, H. H. Lamb and F. Li, *Appl. Catal., B*, 2018, **232**, 77–85.

19 Y. Gao, F. Haeri, F. He and F. Li, *ACS Catal.*, 2018, **8**, 1757–1766.

20 M. Zhou and H. Wang, *JACS Au*, 2022, **2**, 188–196.

21 X. Wang, L. Wan, Z. Wang, X. Liu, Y. Gao, L. Wang, J. Liu, Q. Guo, W. Hu and J. Yang, *J. Phys. Chem. Lett.*, 2022, **13**, 6532–6540.

22 R. Zhang, H. Wang, S. Tang, C. Liu, F. Dong, H. Yue and B. Liang, *ACS Catal.*, 2018, **8**, 9280–9286.

23 Y. Jiang, W. Zhao, S. Li, S. Wang, Y. Fan, F. Wang, X. Qiu, Y. Zhu, Y. Zhang and C. Long, *J. Am. Chem. Soc.*, 2022, **144**, 15977–15987.

24 L. Song, R. Zhang, C. Zhou, G. Shu, K. Ma and H. Yue, *Chem. Commun.*, 2023, **59**, 478–481.

25 F. Li, B. Wang, X. Chen, Y. Lai, T. Wang, H. Fan, X. Yang and Q. Guo, *JACS Au*, 2022, **2**, 2607–2616.

26 Z. Ren, Q. Guo, C. Xu, W. Yang, C. Xiao, D. Dai and X. Yang, *Chin. J. Chem. Phys.*, 2012, **25**, 507–512.

27 E. Lira, J. Ø. Hansen, P. Huo, R. Bechstein, P. Galliker, E. Lægsgaard, B. Hammer, S. Wendt and F. Besenbacher, *Surf. Sci.*, 2010, **604**, 1945–1960.

28 I. Sokolović, M. Reticcioli, M. Čalkovský, M. Wagner, M. Schmid, C. Franchini, U. Diebold and M. Setví, *Proc. Natl. Acad. Sci. U. S. A.*, 2020, **117**, 14827–14837.

29 L. Chen, R. S. Smith, B. D. Kay and Z. Dohnálek, *Surf. Sci.*, 2016, **650**, 83–92.

30 M. A. Henderson, W. S. Epling, C. H. Peden and C. L. Perkins, *J. Phys. Chem. B*, 2003, **107**, 534–545.

31 R. T. Zehr and M. A. Henderson, *Surf. Sci.*, 2008, **602**, 2238–2249.

32 R. Sun, X. Liu, X. Chen, L. Che, X. Yang and Q. Guo, *J. Phys. Chem. Lett.*, 2022, **13**, 801–807.

33 J. Xie, R. Jin, A. Li, Y. Bi, Q. Ruan, Y. Deng, Y. Zhang, S. Yao, G. Sankar and D. Ma, *Nat. Catal.*, 2018, **1**, 889–896.

34 J. J. Lin, D. W. Hwang, S. Harich, Y. T. Lee and X. Yang, *Rev. Sci. Instrum.*, 1998, **69**, 1642–1646.

35 J. T. Grant, C. A. Carrero, F. Goeltl, J. Venegas, P. Mueller, S. P. Burt, S. Specht, W. McDermott, A. Chieregato and I. Hermans, *Science*, 2016, **354**, 1570–1573.

36 J. Ø. Hansen, R. Bebensee, U. Martinez, S. Porsgaard, E. Lira, Y. Wei, L. Lammich, Z. Li, H. Idriss and F. Besenbacher, *Sci. Rep.*, 2016, **6**, 21990.

37 Z. Ma, Q. Guo, X. Mao, Z. Ren, X. Wang, C. Xu, W. Yang, D. Dai, C. Zhou and H. Fan, *J. Phys. Chem. C*, 2013, **117**, 10336–10344.

38 Y. K. Kim, B. D. Kay, J. White and Z. Dohnálek, *Catal. Lett.*, 2007, **119**, 1–4.

39 F. Li, X. Chen, Y. Lai, T. Wang, X. Yang and Q. Guo, *J. Phys. Chem. Lett.*, 2022, **13**, 9186–9194.

40 T. L. Thompson and J. T. Yates, *J. Phys. Chem. B*, 2005, **109**, 18230–18236.

41 T. L. Thompson and J. T. Yates, *J. Phys. Chem. B*, 2006, **110**, 7431–7435.

42 Y. Lai, Y. Zeng, X. Chen, T. Wang, X. Yang and Q. Guo, *J. Phys. Chem. C*, 2023, **127**, 1863–1869.

43 J. F. Weaver, C. Hakanoglu, A. Antony and A. Asthagiri, *Chem. Soc. Rev.*, 2014, **43**, 7536–7547.

44 V. Fung, F. F. Tao and D.-e. Jiang, *Phys. Chem. Chem. Phys.*, 2018, **20**, 22909–22914.

45 C.-C. Wang, S. S. Siao and J.-C. Jiang, *J. Phys. Chem. C*, 2012, **116**, 6367–6370.

46 V. Fung, G. Hu, F. Tao and D. E. Jiang, *ChemPhysChem*, 2019, **20**, 2217–2220.

47 M. A. Henderson, *Surf. Sci. Rep.*, 2011, **66**, 185–297.

48 Q. Zhang, Y. J. Li, H. F. Wen, Y. Adachi, M. Miyazaki, Y. Sugawara, R. Xu, Z. H. Cheng, J. N. Brndiar and L. Kantorovich, *J. Am. Chem. Soc.*, 2018, **140**, 15668–15674.

49 J. Mullins, *J. Chem. Educ.*, 2012, **89**, 834–836.

50 D. Wilson, D. Sporleder and M. White, *J. Phys. Chem. C*, 2013, **117**(18), 9290–9300.

51 C. Walenta, S. Kollmannsberger, C. Courtois, M. Tschurl and U. Heiz, *Phys. Chem. Chem. Phys.*, 2018, **20**, 7105–7111.

52 D. Wilson, D. Sporleder and M. White, *Phys. Chem. Chem. Phys.*, 2012, **14**, 13630–13637.

53 X. Rozanska and J. Sauer, *Int. J. Quantum Chem.*, 2008, **108**, 2223–2229.

54 C. Coperet, *Chem. Rev.*, 2010, **110**, 656–680.

55 G.-L. Dai, Z.-P. Liu, W.-N. Wang, J. Lu and K.-N. Fan, *J. Phys. Chem. C*, 2008, **112**, 3719–3725.

56 Y. Lai, Y. Zeng, F. Li, X. Chen, T. Wang, X. Yang and Q. Guo, *J. Phys. Chem. Lett.*, 2023, **14**, 6286–6294.

